Structural Features of a Three-Stranded DNA Junction Containing a C-C Junctional Bulge†

Mark A. Rosen‡ and Dinshaw J. Patel*,‡,§

Department of Biochemistry and Molecular Biophysics, College of Physicians and Surgeons, Columbia University, New York, New York 10032, and Cellular Biochemistry and Biophysics Program, Memorial Sloan-Kettering Cancer Center, 1275 York Avenue, New York, New York 10021

Received December 9, 1992; Revised Manuscript Received April 8, 1993

ABSTRACT: We have examined the stability of junctional base pairs in a three-way DNA junction with two unpaired cytidine residues at the branch point using two-dimensional nuclear Overhauser effect spectroscopy in H_2O solution. Our data directly support the presence of two of the three junctional Watson–Crick base pairs, with indirect support for the third as well. These results complement the data presented in the preceding paper, where we examined the nonexchangeable proton resonance assignments of three-way DNA junctions from NOESY data in D_2O solution. We have incorporated the NOE data from both sets of experiments, using this information as input for a combined distance geometry (DG) and simulated annealing (SA) protocol designed to derive three-dimensional structures of the junction molecule consistent with the NMR data. Although the data does not allow us to derive a unique solution for the structure of the molecule, certain conformational features are invariably present in our models. We demonstrate the existence of a preferred, pair-wise stacking arrangement between two of the three helices in the junction. Furthermore, the remaining duplex stem is situated so that it always forms an acute angle with just one of the arms from the quasi-continuous helix. The unpaired residues provide an extended backbone segment linking two of the helices together. The first unpaired base on the 5′ end loops out from the interior of the molecule to reside along the minor groove of one helix. The second is located within the interior of the molecule, stacking below one of the junctional base pairs. Our findings suggest that junctional base pair stacking is an important determinant in the conformation of multistranded nucleic acid junctions. In three-way junctions, the presence of unpaired bases at the branch point provides a relief from covalent constraints that would otherwise prevent the simultaneous realization of both base pairing and base pair stacking within the branch point of the molecule.

In the preceding paper in this issue, we have presented the results of a nuclear magnetic resonance study of three-stranded DNA junctions containing unpaired bases at the branch point site. We have shown that a stable junction of this type can be made from two DNA oligomers, in which two of the three strands of the junction are connected by a hairpin loop. We have made three such junction molecules which differ only in the identity of the unpaired bases (C-C, A-A, or I-I).

Our results indicate that the nature of the unpaired bases can affect certain aspects of molecular structure. Unpaired pyrimidines appear to loop out from the interior of the DNA helices, whereas unpaired purines prefer locations within the interior of the molecules. These tendencies may explain the strong conservation of certain unpaired bases in naturally occurring three-way RNA junctions, such as in the 5S RNA molecule (Fox & Woese, 1975; Wolters & Erdmann, 1988). The conformational preferences of the unpaired bases within this junction may play a role in determining the global structure of the molecule. In support of this postulate, it has been shown that the identity of these bases is important for high-affinity binding of TFIIIA, a zinc-finger protein which recognizes two of the three helices at the junction site of the RNA molecule (Romaniuk, 1989; Baudin et al., 1991).

Helical stacking is thought to be an important conformational feature of multistranded nucleic acid junctions. This is especially true of the four-stranded, or Holliday, junction in DNA, an intermediate in genetic recombination (Meselson & Radding, 1975; Orr-Weaver et al., 1981). The currently favored structural model of Holliday junctions consists of two pairs of semicontinuous helices in an "X" configuration (Sigal & Alberts, 1972; von Kitzing et al., 1990). Within three-way DNA junctions, no such stacking interactions are thought to exist (Duckett & Lilley, 1990). However, it has recently been shown that unpaired bases at the branch point have a stabilizing effect on three-way DNA junctions (Leontis et al., 1991). It is possible that without these additional bases it is sterically impossible to form a pair-wise helical stack without disrupting Watson–Crick base pairs adjacent to the branch point.

In this report, we present the results of a more detailed structural study of a three-way DNA junction with two unpaired cytidine residues in one strand. The sequence and numbering scheme of this molecule are shown in Chart I. The junction is named "J3CC" due to the presence of two unpaired cytidine bases at the branch point. Two of the strands within the junction are connected by a four-base loop, 5′-TTTA-3′. This DNA tetraloop is unusually stable and possesses a unique conformation in solution (Blommers et al., 1989, 1991). We have investigated the stability of the three internal base pairs in this molecule through proton nuclear magnetic resonance spectroscopy in solution. By combining these NOESY results in H_2O solution with our prior results in D_2O solution, we

† This research was supported by NIH Grant GM34504 to D.P.M.R was supported by NIH Medical Scientist Training Program Training Grant 5-T32-GM07376. The NMR spectrometers were purchased from funds donated by the Robert Wood Johnson Trust toward setting up an NMR center in the Basic Medical Sciences at Columbia University. We acknowledge the use of the Molecular Modeling Facility for Molecular Biology at Columbia University, supported in part by NSF Grant DIR-8720229.

‡ Columbia University.

§ Memorial Sloan-Kettering Cancer Center.

0006-2960/93/0432-6576$04.00/0

Chart I

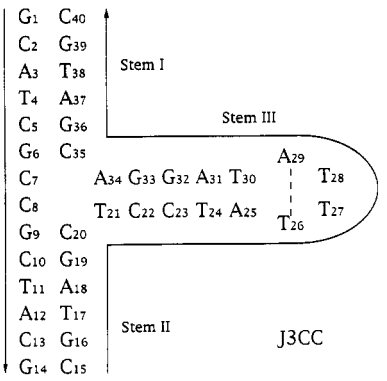

have determined a structural model of J3CC, demonstrating the presence of a pair-wise stacking interaction between two of the three helices within the junction.

MATERIALS AND METHODS

DNA Synthesis and Preparation of NMR Samples. DNA oligomers were synthesized on solid supports (10-μmol scale) on an Applied Biosystems 391 automated DNA synthesizer using standard phosphoramidite chemistry. Purification of oligomers to the Na^+-DNA salt was as described previously (Rosen & Patel, 1993). Oligomer strand concentrations were quantitated by ultraviolet absorption at 260 nm, using extinction coefficients calculated by the nearest-neighbor model (Fasman, 1975).

NMR samples were prepared by mixing equimolar amounts of the two strands in 0.4 mL of NMR buffer (10 mM sodium phosphate, pH 6.2, with 200 mM NaCl and 0.1 mM EDTA). Strands were annealed prior to NMR experiments by heating the sample to 80 °C for 15 min followed by slow cooling to room temperature. The samples were then lyophilized to dryness and redissolved in 0.4 mL of 10% D_2O/90% H_2O. DNA concentration was 2–3 mM in each strand.

Proton Nuclear Magnetic Resonance Spectroscopy. One-dimensional ^{1}H-NMR spectra in H_2O buffer were recorded on a Bruker AM-400WB spectrometer. Solvent suppression was achieved through the use of a "jump-and-return" pulse sequence (Plateau & Gueron, 1982). Two-dimensional NOESY spectra were acquired on a Bruker AM-500 spectrometer in the phase-sensitive mode (States et al., 1982). Acquisition parameters were identical to those previously described (Rosen & Patel, 1993). The NOESY spectra in H_2O buffer were acquired with a 70–70–J&R pulse scheme. NOESY data sets were processed with a 30–45° shifted squared sinebell in each dimension. All spectra were referenced relative to an internal sodium 4,4-dimethyl-4-silapentane-1-sulfonate (DSS) standard.

Structural Determination of the Three-Way Junction. For deriving a structural model of the three-way DNA junction consistent with our NMR data, we elected to use a combination of distance geometry (DG) and simulated annealing (SA). The combined DG/SA protocol we used is described in detail in the Results section. The DG routine of the X-PLOR modeling package, version 3.0 (Brunger, 1993) was used, with random four-atom metrization (Kuszewski et al., 1992). Molecular dynamics simulations were performed *in vacuo* using an all-atom force field derived from CHARMM (Nilsson & Karplus, 1986). Explicit hydrogen-bonding forces were included for all residues within the double-stranded regions of the molecule. Counterion effects were included by reducing the phosphate charges, and solvent shielding was approximated by a distance-dependent dielectric, $\epsilon = r$. All computations were carried out on a Convex C2 computer. Structural models were visualized on a Silicon Graphics IRIS-4D workstation equipped with the graphics software INSIGHTII (Biosym, Inc., San Diego, CA). Helicoidal parameters were determined using the CURVES algorithm (Lavery & Sklenar, 1988, 1989). Distribution plots of helicoidal parameters were prepared with the DIALS and WINDOWS program (Ravishanker et al., 1989).

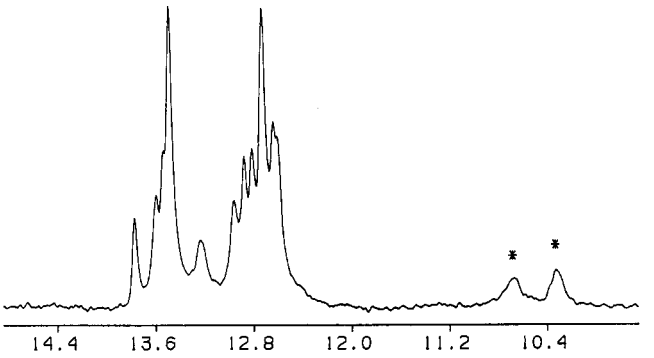

FIGURE 1: Downfield portion (10.0–14.5 ppm) of the proton NMR spectrum of J3CC in H_2O buffer (10 mM sodium phosphate, pH 6.2, with 200 mM NaCl and 0.1 mM EDTA) at 25 °C. The spectrum is referenced relative to an internal DSS standard. The two broad resonances marked with asterisks belong to the exposed T(imino) protons from the loop residues T27 and T28.

RESULTS

One-Dimensional Proton NMR Spectroscopy of J3CC in H_2O. The downfield portion (10.0–14.5 ppm) of the one-dimensional proton NMR spectrum of J3CC in H_2O buffer (10 mM sodium phosphate, pH 6.2, with 200 mM NaCl and 0.1 mM EDTA) at 25 °C is shown in Figure 1. In DNA, imino protons (NH1 of guanine and NH3 of thymine) resonate between 10 and 15 ppm, depending on whether these protons are hydrogen-bonded within a base pair or are exposed to solvent. The two broad resonances marked by asterisks between 10 and 11 ppm are typical for unpaired thymine imino protons. They belong to T27 and T28, the second and third thymines of the hairpin loop (Blommers et al., 1989). Further downfield, there are a number of sharp resonances between 12 and 14 ppm. Resonances in this region arise from imino protons that participate in hydrogen-bonded base pairing. The broader resonance at 13.31 ppm is another fast-exchanging imino proton. On the basis of its chemical shift and exchange characteristics, we assign this to the first thymine residue in the hairpin loop, T26. This residue was shown (Blommers et al., 1989) to participate in a Hoogsteen base pair with the fourth residue in the loop, A29. The NMR evidence here and in D_2O (Rosen & Patel, 1993) suggests that the 5′-TTTA-3′ hairpin loop behaves similarly within either the J3CC junction studied here or the stem-loop hairpin molecule studied by Hilbers and colleagues (Blommers et al., 1989, 1991).

The extensive overlap in the downfield portion of the spectrum in Figure 1 precludes us from quantifying the number of imino proton resonance lines between 12 and 14 ppm. However, it is clear that there are more base-paired imino protons than can be accounted for simply through pairing within the stem region of the hairpin loop strand. The one-dimensional spectrum of this strand alone (data not shown) has fewer resonance lines in this region, with several additional broad peaks or humps between 10 and 12 ppm. The large

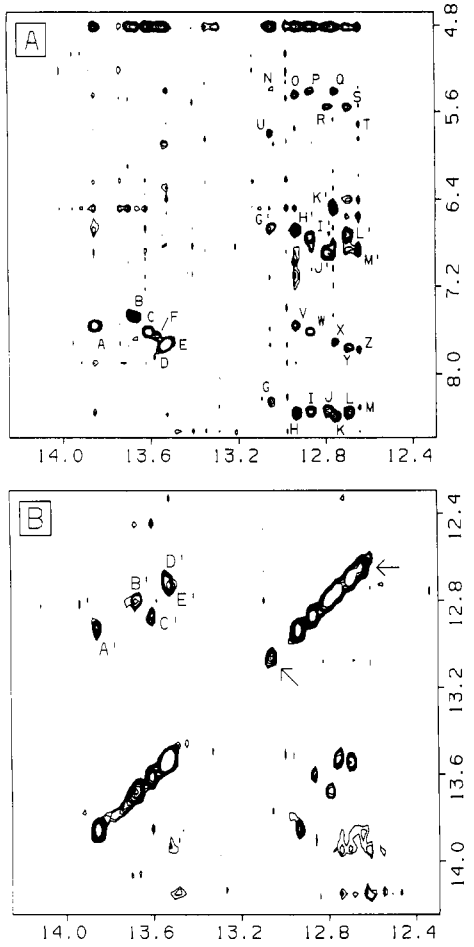

FIGURE 2: Expanded contour plots of the NOESY experiment (180-ms mixing time) on J3CC in H_2O buffer with 100 mM NaCl at 20 °C. The imino–base/amino (panel A) and the imino–imino (panel B) regions of the spectrum are shown. Assignments for labeled cross peaks are as follows: (A) T11(imino)–A18(H2), (A′) T11(imino)–G19(imino), (B) T24(imino)–A31(H2), (B′) T24(imino)–G32-(imino), (C) T17(imino)–A12(H2), (C′) T17(imino)–G16(imino), (D) T4(imino)–A37(H2), (D′) T4(imino)–G36(imino), (E) T38-(imino)–A3(H2), (E′) T38(imino)–G39(imino), (F) T30(imino)–A25(H2), (G,G′) G9(imino)–C20(amino, b/e), (H,H′) G19(imino)–C10(amino, b/e), (I,I′) G16(imino)–C13(amino, b/e), (J,J′) G32(imino)–C23(amino, b/e), (K,K′) G39(imino)–C2(amino, b/e), (L,L′) G36(imino)–C5(amino, b/e), (M,M′) G33(imino)–C22-(amino, b/e), (N) G9(imino)–C20(H5), (O) G19(imino)–C10(H5), (P) G16(imino)–C13(H5), (Q) G39(imino)–C2(H5), (R) G32-(imino)–C23(H5), (S) G36(imino)–C5(H5), (T) G33(imino)–C22-(H5), (U) G9(imino)–C8(H5), (V) G19(imino)–A18(H2), (W) G16(imino)–A12(H2), (X) G39(imino)–A3(H2), (Y) G36(imino)–A37(H2), (Z) G33(imino)–A34(H2). The term "b/e" refers to the hydrogen-bonded and the exposed cytosine amino protons, respectively.

number of sharp imino resonances between 12 and 14 ppm in Figure 1 indicates that at least some of the bases within stems I and II of J3CC participate in Watson–Crick base pairing.

Two-Dimensional Proton NMR Spectroscopy of J3CC in H_2O. In order to quantify the number of base pairs within J3CC, we ran NOESY experiments in H_2O buffer. For these experiments, the NaCl concentration was decreased to 100 mM in order to produce sharper imino proton resonance lines. The imino–imino and imino–H2/amino regions of the NOESY experiment at 20 °C are shown in Figure 2. In the imino–H2/amino region (panel A), six strong cross peaks on the left (labeled A–F) represent NOEs for the short T(imino)–A(H2) distance within AT base pairs. On the right, seven pairs of resonances are labeled G–M and G′–M′. These correspond to seven GC base pairs, with NOE connectivities seen from the guanine imino proton to the hydrogen-bonded and solvent-exposed cytidine amino protons. The presence of these base pairs is confirmed by the observation of strong NOEs between the geminal cytidine amino protons. We also note the presence of spin diffusion cross peaks between the G(imino) and C(H5) protons (cross peaks N–T, Figure 2A).

At 20 °C, fraying of short DNA duplexes allows the imino protons from terminal base pairs to exchange rapidly with solvent. As a result of this exchange process, these imino proton resonance lines are quite broad and are generally unobservable in NOESY experiments. Inspection of the sequence of J3CC shows that, after discounting the two terminal GC base pairs (G1·C40 and G14·C15), along with the fast-exchanging T26·A29 Hoogsteen base pair, one is left with seven AT and eight GC base pairs in the molecule. We have noted that, at 20 °C, six AT and seven GC base pairs are evident from the interstrand NOESY cross peaks seen in Figure 2. We can therefore confirm, even without sequential assignments for any of these exchangeable proton resonances, that at least one of the three junctional base pairs of J3CC is intact at 20 °C. This analysis complements the findings of Wemmer et al. (1985) that internal base pairs in junctional complexes of DNA may be stable at ambient temperatures.

In the imino–imino region of Figure 2 (panel B), there are five NOE connectivities, labeled A′–E′, between T(imino) and G(imino) protons. Inspection of the sequence of J3CC indicates that there are six (GC)-(AT) steps in the junction. Clearly one possible G(imino)–T(imino) connectivity is not observable or is overlapped under these conditions. The most likely candidate would be the connectivity between the imino protons of T21 and G33 in stem III, since this is the only (GC)-(AT) step involving one of the junctional base pairs. Two diagonal G(imino) peaks that fail to show an NOE to any T(imino) proton are indicated with arrows in the figure. After excluding the two terminal guanine residues, G1 and G14, the only remaining candidates for these two imino resonances are G6, G9, and G33.

By correlating G(imino)–C(H5) and T(imino)–A(H2) cross peaks with previous nonexchangeable proton assignments (Rosen & Patel, 1993), we have assigned all seven guanine imino and six thymine imino protons of J3CC visible in the NOESY spectrum at 20 °C. These assignments were confirmed by the presence of sequential NOEs between imino protons (cross peaks A′–E′, Figure 2B) and between G(imino) and A(H2) protons (cross peaks V–Z, Figure 2A). Of special note is the presence of the G9(imino)–C20(amino) cross peaks (G and G′, Figure 2A), confirming the presence of this junctional base pair in J3CC at 20 °C. Interestingly, the G9(imino)–C20(H5) cross peak is quite weak (peak N, Figure 2A), and instead we see a strong cross peak from this imino proton to the H5 proton of C8 at 5.79 ppm (peak U, Figure 2A). This unusually strong connectivity reveals that the bulged base C8 stacks with the G9·C20 base pair, but that the C8-G9 base step is unusual, with C8 sliding in the direction of its major axis beneath the adjoining base pair.

Of the three junctional base pairs, G6·C35, G9·C20, and T21·A34, the G9·C20 pair is the only one we can demonstrate directly in the NOESY spectrum at 20 °C. However, we do note the presence in Figure 2A of cross peak Z, between the G33(imino) proton and a proton at 7.77 ppm. The chemical shift of this resonance suggests that it is the H2 proton of A34. However, no corresponding NOE between A34(H2) and T21-(imino) is seen. We conclude from this that A34 stacks under G33. However, under the conditions of the experiment, the

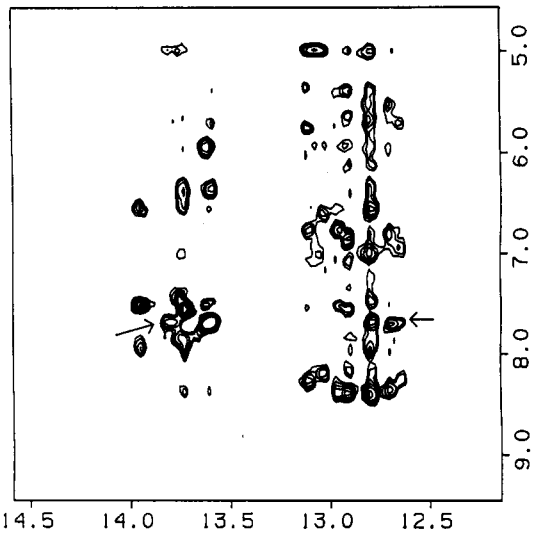

FIGURE 3: Expanded contour plot of a NOESY spectrum (180-ms mixing time) of J3CC in H_2O buffer with 100 mM NaCl at 0 °C. The DNA concentration was one-half that used for the NOESY experiment at 20 °C in Figure 2. The imino–base/amino region of the spectrum is shown. Arrows mark the positions of the new T21-(imino)–A34(H2) NOE cross peak (left) and the G33(imino)–A34-(H2) NOE (right).

T21·A34 base pair, if present, is weak, and the T21(imino) proton must undergo rapid exchange with solvent.

To examine this question further, we ran an additional NOESY experiment on J3CC in H_2O buffer, this time at 0 °C. An expanded contour plot of this experiment detailing the imino to base/amino region is shown in Figure 3. In general the results are quite similar to those of the NOESY experiment at 20 °C, though the resolution has decreased considerably due to the broader resonance line widths at the lower temperature. One striking new feature of this spectrum is the appearance of an additional T(imino)–A(H2) NOE cross peak (left arrow). This cross peak aligns with the A34-(H2) proton, as seen by the position of the G33(imino)–A34-(H2) cross peak (right arrow). Therefore this cross peak must represent the T21(imino)–A34(H2) NOE connectivity, indicating an intact Watson–Crick base pair at this position of the molecule. We now have direct evidence that two of the three possible base pairs adjacent to the branch point are stable in J3CC. There are no observable NOEs to the G6-(imino) proton in the 0 °C NOESY spectrum. However, this does not necessarily imply that G6·C35 is not paired in the junction. The one-dimensional NMR spectrum of J3CC in H_2O buffer at 0 °C contains no broad peaks between 11 and 12 ppm that would indicate the presence of an unpaired guanine imino proton. Furthermore, in the 0 °C NOESY spectrum, we do see an extra diagonal peak in the guanine imino region at 13.21 ppm. This imino resonance does not belong to either G1 or G14, the two terminal guanines, and therefore could be the G6(imino) proton. To summarize, within the J3CC junction we see direct evidence that two of the three possible junctional base pairs are formed, as well as indirect evidence for the third.

Table I lists the chemical shift assignments of the exchangeable imino and amino protons, as well as those of the nonexchangeable A(H2) and C(H5) protons, of J3CC in H_2O buffer at 0 °C.

Modeling the Three-Dimensional Structure of J3CC. The NOESY/H_2O data from the J3CC junction, along with the previous NOESY/D_2O data (Rosen & Patel, 1993), provide a core of information upon which we attempted to build a structural model of the three-way DNA junction. To develop

Table I: Proton Chemical Shift Assignments for J3CC in H_2O Buffer at 0 °C, pH 6.2

	chemical shifts (ppm)					
base pair	NH3	NH1	NH4(b)[a]	NH4(e)[a]	H2	H5
			Stem I			
G1·C40		13.03	8.19	6.61		
C2·G39		12.78	8.40	6.56		5.38
A3·T38	13.58				7.68	
T4·A37	13.60				7.71	
C5·G36		12.69	8.36	6.81		5.52
G6·C35						
			Bulge			
C7						
C8						5.75
			Stem II			
G9·C20		13.10	8.26	6.77		5.36
C10·G19		12.95	8.36	6.77		5.41
T11·A18	13.94				7.51	
A12·T17	13.71				7.56	
C13·G16		12.90	8.39	6.86		5.38
G14·C15		12.90	8.15	7.08		5.90
			Stem III			
T21·A34	13.79				7.69	
C22·G33		12.64	8.25	6.94		5.70
C23·G32		12.79	8.39	6.99		5.51
T24·A31	13.74				7.47	
A25·T30	13.61				7.51	
T26·A29	13.30					

[a] The letters "b" and "e" refer to the hydrogen-bonded and the exposed cytosine amino protons, respectively.

this model, we began with a set of working hypotheses. First, we assumed that each of the three component helices of the junction resembled a B-form DNA duplex. Second, all three junctional Watson–Crick base pairs of the molecule, even if not explicitly visible in the NOESY spectra in H_2O, were assumed to be intact. Finally, we postulated that the component helices and bulged bases of the three-way junction could be joined together in a sterically reasonable manner, consistent with our NOE data, without the necessity of deforming the sugar–phosphate backbones of the helical segments. We employed a two-stage procedure for obtaining structural models. Distance geometry (DG) was used to generate initial models of the junction, followed by simulated annealing (SA) to regularize the structures.

We began by constructing B-DNA helices of the appropriate sequence for each of the three stems within the junction. The 5′-TTTA-3′ hairpin loop was then constructed based on the coordinates provided by C. Hilbers (University of Nijmegen, Netherlands). This loop was manually joined to the third helical stem. Each of the three "subdomains" of J3CC was then subjected to 500 steps of conjugate gradient minimization prior to DG calculations.

We next proceeded to embed substructures of the junction using a reduced atom set consisting of P, C2′, N7, and N1 for purines; P, C2′, and C5 for cytidines; and P, C2′, and C5M (the methyl carbon) for thymidines and the 5-methylcytidine residue. This selection reduced the number of atoms to embed from over 1200 to 138, a manageable number for the purposes of generating a large number of substructures. We chose to include the 5-methylcytidine residue due to the additional structural information derived from NOEs to these methyl protons. The three helical domains were used as fixed groups to direct the embedding procedure, with a distance allowance of ±0.5 Å.

NOE constraints were included in the distance matrix by reducing the set of proton pairs to a smaller set of heavy-atom pairs chosen from the embedded atoms. All sugar protons

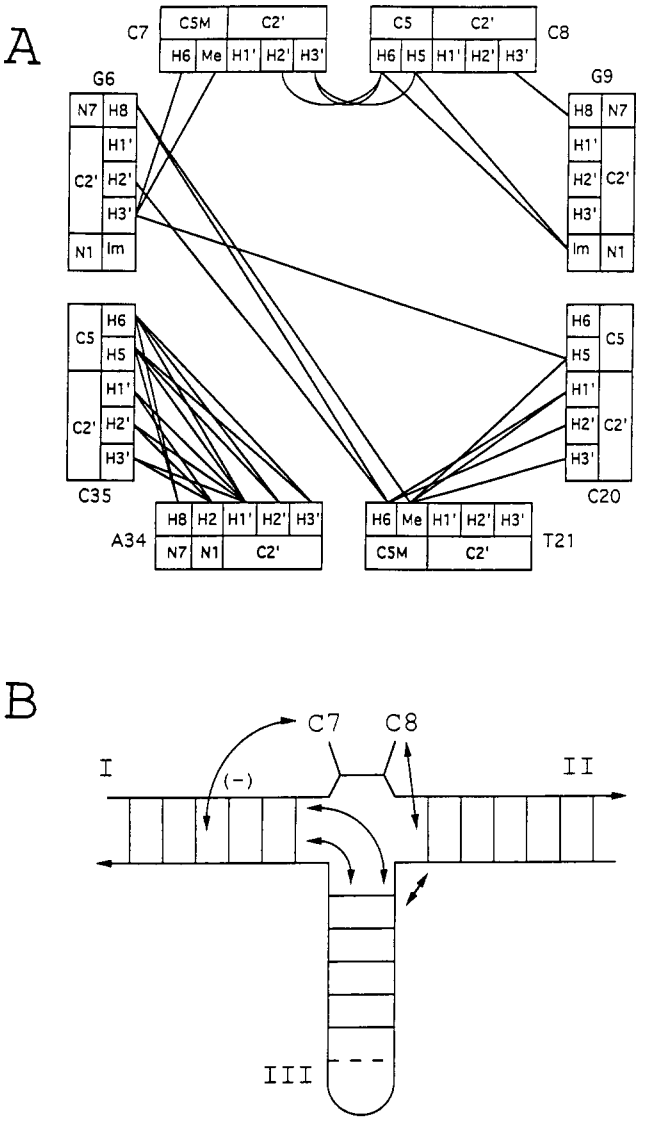

FIGURE 4: Schematic illustration of the NOE restraints among the junctional bases of J3CC. (A) Proton–proton NOEs at the branch point. All positive NOEs are shown equally, whereas negative NOE information is not included in the diagram. The specific protons involved in each NOE connectivity are shown on the inner face of the bases. The heavy atoms used to represent the various proton–proton interactions within the bounds matrix of the distance geometry calculations are indicated on the outer face. Only NOEs involving two protons from junctional bases are shown. Hydrogen-bonding restraints for the base pairs G6·C35, G9·C20, and T21·A34 were also included. (B) Secondary structure of J3CC showing the three duplex stems and the two unpaired bases at the branch point. Arrows indicate critical NOE restraints that help to define the tertiary structure of the molecule. The negative sign above stem I indicates that C7 lies along the minor groove of that helix.

were represented by the C2′ atom; base protons (major groove), by the C5, CM5, or N7 atom; and imino or H2 protons, by the N1 atom. For observable NOEs involving protons from junctional bases, we assigned a distance range of 2.0–7.0 Å between the parent heavy atoms. For selected proton pairs in which an NOE connectivity was clearly absent, we assigned a distance of 5.0 Å or greater to the appropriate heavy-atom pairs. Within the NOESY spectra of both the original and the methylated J3CC junction, certain NOE cross peaks could be clearly resolved only in the original molecule, whereas others were seen only in the methylated one. The NOE information therefore represents a composite picture of the two junction molecules. Figure 4 schematically illustrates some of this NOE information within the branch point of the junction.

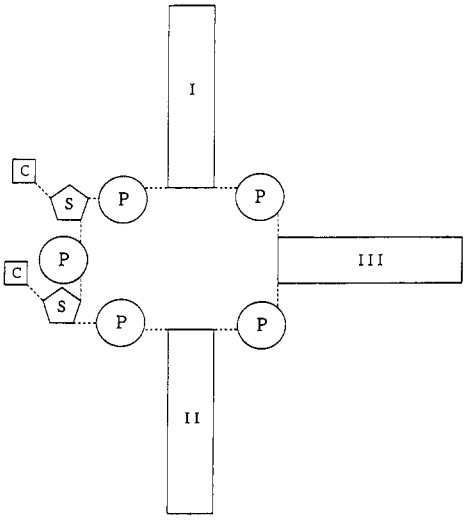

FIGURE 5: Schematic diagram delineating the division of J3CC into twelve rigid groups. The three duplex stems are labeled by Roman numerals. Phosphate groups are represented by a letter "P" in a circle. For the unpaired cytidine residues, additional rigid groups were formed from the base (C) and sugar (S) moieties. The O5′ atoms of junctional bases were included within the neighboring phosphate groups; O3′ atoms remained with the sugar or helical stem groups. This arrangement allowed for free rotation about all backbone dihedral angles at the branch point, except for the δ angle within the deoxyribose rings.

Embedded substructures were screened for proper chirality by checking the handedness of each of the three component helices in the junction. We found that many embedded substructures were generated with a combination of left- and right-handed helices. Only those embeds that produced three helices of identical chirality were accepted, with enantiomeric inversion applied where appropriate. Complete molecular coordinates were then obtained by individually fitting the template helices and the free cytidine residues onto the embedded substructures.

Our initial embeds frequently resulted in compact structures that, when regularized, produced junction models with severe van der Waals (vdW) clashes. Most often, the models contained "knotted" helices, in which the backbone from one helix would pass through the interior of another. Such results are frequently encountered when performing DG calculations on nucleic acid molecules with a reduced atom set (Hubbard & Hearst, 1991). In order to avoid this complication, we increased the van der Waals radii of the embedded atoms by a factor of 3. We found this increase optimal in order to avoid knotted helices. These increased vdW radii did not disturb the integrity of the helical domains themselves, as the DG algorithm overrode the repulsive vdW interactions between atoms within fixed groups.

In junction models derived using these increased vdW radii, the three helical domains were separated in space by large gaps. We therefore employed an extended simulated annealing protocol to regularize the structures, using rigid-body dynamics to maintain the integrity of the helical domains during the molecular dynamics simulations at high temperature. The molecule was divided into twelve rigid units: one from each of the helical stems, three (base, sugar, and phosphate) from each of the unpaired cytidines, and three additional phosphate groups spanning the branch point of the junction. These last three units were included as separate groups in order to ensure free rotation about the backbone dihedral angles at the junctional base steps. The division of the J3CC molecule into twelve rigid domains is shown schematically in Figure 5.

Table II: Simulated Annealing Protocol for Regularization of Distance Geometry Structures

general parameters (except where noted)
- rigid-body restraints maintained throughout dynamics
- dynamics time step set to 1 fs
- atomic masses uniformly set to 100 amu
- frictional coefficient set to 100
- nonbonded distance cutoff set to 4.5 Å
- soft vdW repulsion term used; electrostatics off

high-temperature phase I (1 ps)
- bond and vdW potentials on
- K_b = 1000 kcal/(mol·Å^2)
- vdW radii scaled by 0.75
- vdW exclusion between 1–2-bonded atoms only
- T_{bath} = 2000 K

high-temperature phase II (1 ps)
- angle potential on
- K_a = 500 kcal/(mol·rad^2)
- T_{bath} = 2000 K

high-temperature phase III (1 ps)
- dihedral, improper, NOE potentials on
- K_i = 500 kcal/(mol·rad^2)
- K_{NOE} starts at 1.0 kcal/(mol·Å^2), scaled to 40.0 kcal/(mol·Å^2) by a factor of 1.45 every 100 fs
- vdW exclusion for 1–2- and 1–3-bonded atoms
- frictional coefficients reduced to 10
- T_{bath} = 2000 K

cooling phase (3 ps)
- vdW radii scaled by 0.9
- vdW exclusion for 1–2-, 1–3-, and 1–4-bonded atoms
- K_{vdW} starts at 0.005 kcal/(mol·Å^2) and is increased by a factor of 1.15 every 78 fs to a final value of 1.0 kcal/(mol·Å^2)
- frictional coefficient starts at 10 and is increased by a factor of 1.06 every 78 fs to a final value of 100
- T_{bath} starts at 2000 K and is decreased by 50 K every 78 fs to a final value of 100 K

minimization (500 steps)
- electrostatic and H-bond potentials on
- vdW radii scaled to normal values
- Lennard-Jones vdW potential used
- nonbonded cutoff distance increased to 11.5 Å
- rigid-body restraints removed
- Watson–Crick hydrogen bonds reinforced with NOE restraints [squared flat-well potential, width = 0.2 Å, $K_{NOE(hb)}$ = 8.0 kcal/(mol·Å^2)]

The SA protocol is presented in detail in Table II. It is loosely based on the "dgsa" method for the regularization of DG structures within X-PLOR (Brunger, 1992; Kuszewski et al., 1992), modified for rigid-body dynamics. Each structure was subjected to 3 ps of high-temperature dynamics followed by 3 ps of gradual cooling. During the last 1 ps at high temperature, the frictional coefficient was lowered, resulting in transient local heating in the system. This was employed to ensure that energetic boundaries could be overcome as the molecule searched for conformations consistent with covalent geometry and NOE information. Frictional drag was gradually increased to its original levels during the cooling phase to help dissipate the excess kinetic energy in the system as the molecule settled into a specific conformation. Each simulation was capped with 500 steps of energy minimization, during which the rigid-body restraints were eliminated in order to relax any energetic strain at the branch point of the molecule.

We ran 50 separate DG/SA simulations to evaluate the conformational space available to the junction molecule. Given the limited number of NOE restraints we were able to impose on the molecule, we expected the results to span a range of three-dimensional geometries. We therefore directed our efforts toward describing the general conformational tendencies seen within the ensemble of junction structures. The 50 structures were sorted according to the final energy of the molecule. A distribution plot of these energies is shown in Figure 6. All but one of the simulations resulted in models that were well-formed with regard to covalent geometry and structural integrity of the helices. The one failed structure was due to unresolvable steric clash between two of the three helices at the branch point.

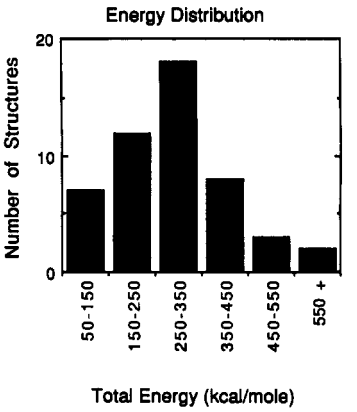

FIGURE 6: Histogram showing distribution of final molecular energies for the 50 DG/SA simulations of J3CC.

Table III: Mean Helical Angles in J3CC Models[a]

	helix pair		
energy (kcal/mol)	I–II	I–III	II–III
50–150 (N = 7)	139.8(15.2)	160.5(6.7)	32.2(8.3)
150–250 (N = 12)	117.8(28.1)	146.9(19.5)	55.6(23.6)
250–350 (N = 18)	129.1(28.0)	135.9(23.6)	53.6(14.5)
350–450 (N = 8)	109.0(19.0)	144.2(25.0)	54.2(20.0)
450–550 (N = 3)	105.7(22.5)	119.2(9.9)	30.5(4.4)
>550 (N = 2)	90.7(13.1)	129.8(33.8)	54.8(24.3)
all (N = 50)	121.7(27.4)	142.1(23.6)	49.8(19.8)
control (N = 10)	110.5(30.7)	132.8(21.3)	58.5(27.0)

[a] Angles are between the best linear axes through the central portion of each stem. Standard deviations for each group are shown in parentheses. Control group refers to simulations run in the absence of NOE restraints.

For each subset of structures identified in Figure 6, we calculated the mean and standard deviation of the angles produced by the three helical axes. In order to avoid the influence of end effects or distortions at the branch point site, these angles were derived from the best linear axes through the central four base pairs of each helix. The results are listed in Table III. Among all of the structures, there is a clear pattern: stems I and III span the largest angle; stems II and III, the smallest; and stems I and II, an intermediate angle. This tendency is particularly true among the group of seven lowest-energy structures in Figure 6.

We also ran a series of control DG/SA simulations in the absence of any NOE restraints. The helix angles within this group of structures are also shown in Table III. Interestingly, the trend seen in the experimental group (i.e., angle{I–III} > angle{I–II} > angle{II–III}) is present in the control calculations as well. However, unlike the experimental group, there is no correspondence between the I–III helical angle and the final energy within the control group.

The seven models with the lowest empirical energy have a narrow distribution of angular values, and we focus the remainder of our analysis on this group. In Figure 7 a ball-and-stick representation of the lowest energy conformation we arrived at for the J3CC junction is shown. The colinear stack between stems I and III, as predicted from the NOE data, can be seen on the right. The third arm, stem II (upper left), forms an acute angle with stem III. This is brought about by an abrupt turn in the sugar–phosphate backbone

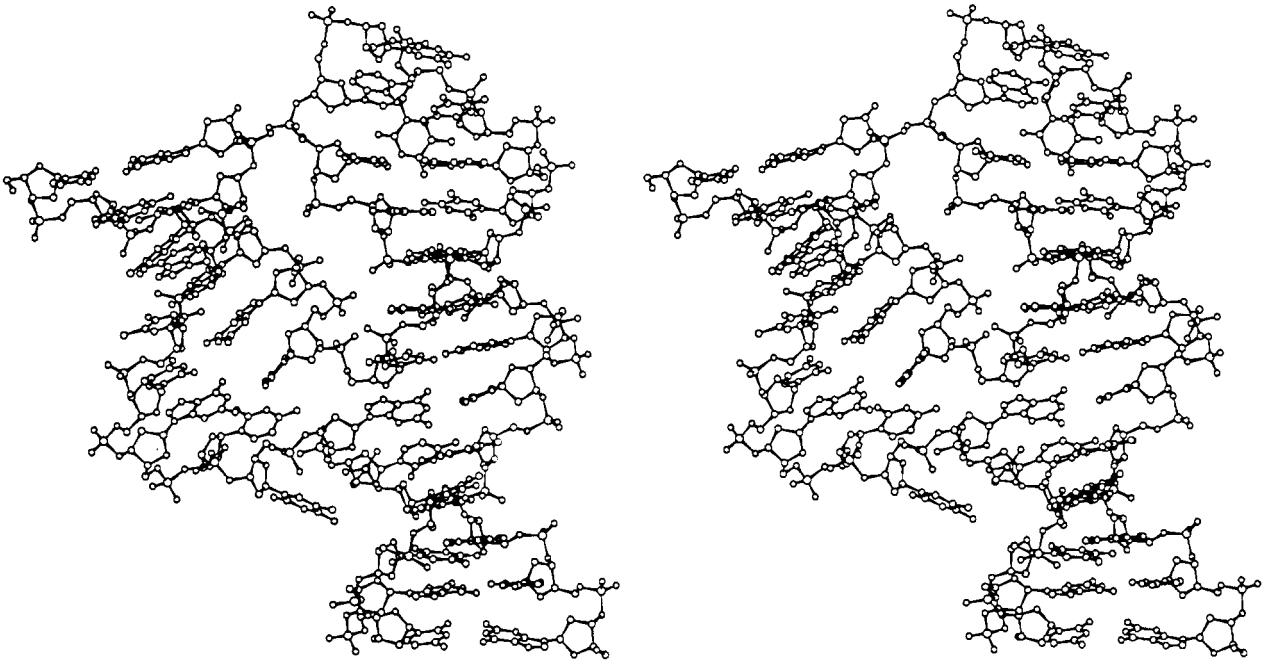

FIGURE 7: Stereoview of a ball-and-stick representation of the lowest energy solution for the structure of the J3CC junction. Hydrogen atoms are omitted for clarity. Stem I is at the bottom, while stem III and the hairpin loop are at the top. The view is into the minor groove of the quasi-continuous helix formed from stems I and III. Stem II is located to the left, pointing slightly away from the viewer. The first unpaired cytosine base, C7, loops out into the minor groove of stem I (bottom left of the figure), while the second base, C8, stacks underneath stem II.

between residues C20 and T21. One of the two bulged bases, the 5-methylcytidine at position 7, lies along the minor groove of stem I, while residue C8 lies beneath the G9·C20 base pair at the base of stem II.

In Figure 8, we show the superposition of helices I and III from the seven lowest energy structures. The view is into the minor groove of the central portion, with stem III in the upper half. Residues T27 and T28 within the hairpin loop of stem III are not included in the figure. Note the highly reproducible alignment of the A34-C35 base step on the right side of the figure. The discontinuous G6-T21 base step, for which fewer NOE restraints were obtainable, is less well constrained. Among these seven structures, the pair-wise atomic root mean square deviation for stems I and III is 1.00 Å. Comparable values for the I–II and II–III helical pairs are 2.91 and 2.95 Å, respectively.

Aside from the break in the backbone between residues G6 and T21, the helix formed from the two stems of the junction is practically indistinguishable from regular B-form DNA. We have examined the helicoidal parameters of this composite helix from each of the lowest energy structures. Though there is a somewhat greater range of values at the junctional base steps, all of the parameters fall within normal limits for B-DNA. Variations at the junctional step are due in part to differences in the direction and magnitude of the angle between the two stems. Graphical plots of these parameters are available in the supplementary material.

Figure 9 shows the superposition of stem II from the seven lowest energy structures, with the position of the neighboring C8 residue highlighted. As can be seen, this residue remains below the G9·C20 base pair but can be variably shifted toward either the major or the minor groove. Given the small number of NOE restraints between these two residues, this conformational variation among our models is not surprising.

Our inability to define the structure of the C7-C8-G9 segment more accurately contributes to the variable position of stem II within the different models of the three-way junction. However, we can draw certain conclusions about the position of the helix in relation to the quasi-continuous I–III helix. As we already described, stem II makes an acute angle with stem III, never with stem I. Only occasionally does the II–III angle even approach 90°. Secondly, among the energetically most favorable structures, stem II is twisted in a right-handed manner relative to the colinear stack of stems I and III. This geometric relationship is pictured in Figure 10. In Figure 10A, the helical axes of stem II from all seven structures are shown against the backbone tracings of the quasi-continuous I–III helices. The twist angle ranges between 0° and 50°. In Figure 10B, stem II from one junction model is shown against a ribbon representation of the entire molecule. Among the 50 DG/SA simulations we performed, molecules with left-handed and right-handed twists were represented equally. However, we found that the energetically most favorable structures were almost exclusively right-handed.

DISCUSSION

Base Pairing at the Branch Point of J3CC. The NOESY spectra of J3CC in H_2O buffer yield information on the status of the base pairs proximate to the branch point site of the three-way DNA junction. In J3CC, there are three such possible base pairs: G6·C35, G9·C20, and T21·A34. The data indicate that the G9·C20 pair is the most stable of the three, clearly present in the NOESY spectrum at 20 °C. In the NOESY spectrum at 0 °C, the T21·A34 base pair can also be seen.

The evidence presented in the H_2O-NOESY spectra directly supports the presence of intact Watson–Crick base pairing for some of the junctional bases in the three-stranded junction. This result complements NMR studies on the status of base pairs in four-stranded DNA junctions (Wemmer et al., 1985; Chen et al., 1993), which provided evidence of junctional base pairing within these molecules as well.

We cannot find any direct evidence for the existence of the G6·C35 base pair within the J3CC junction. However, the absence of any broad resonance lines between 11 and 12 ppm suggests that the G6(imino) proton may be hydrogen-bonded

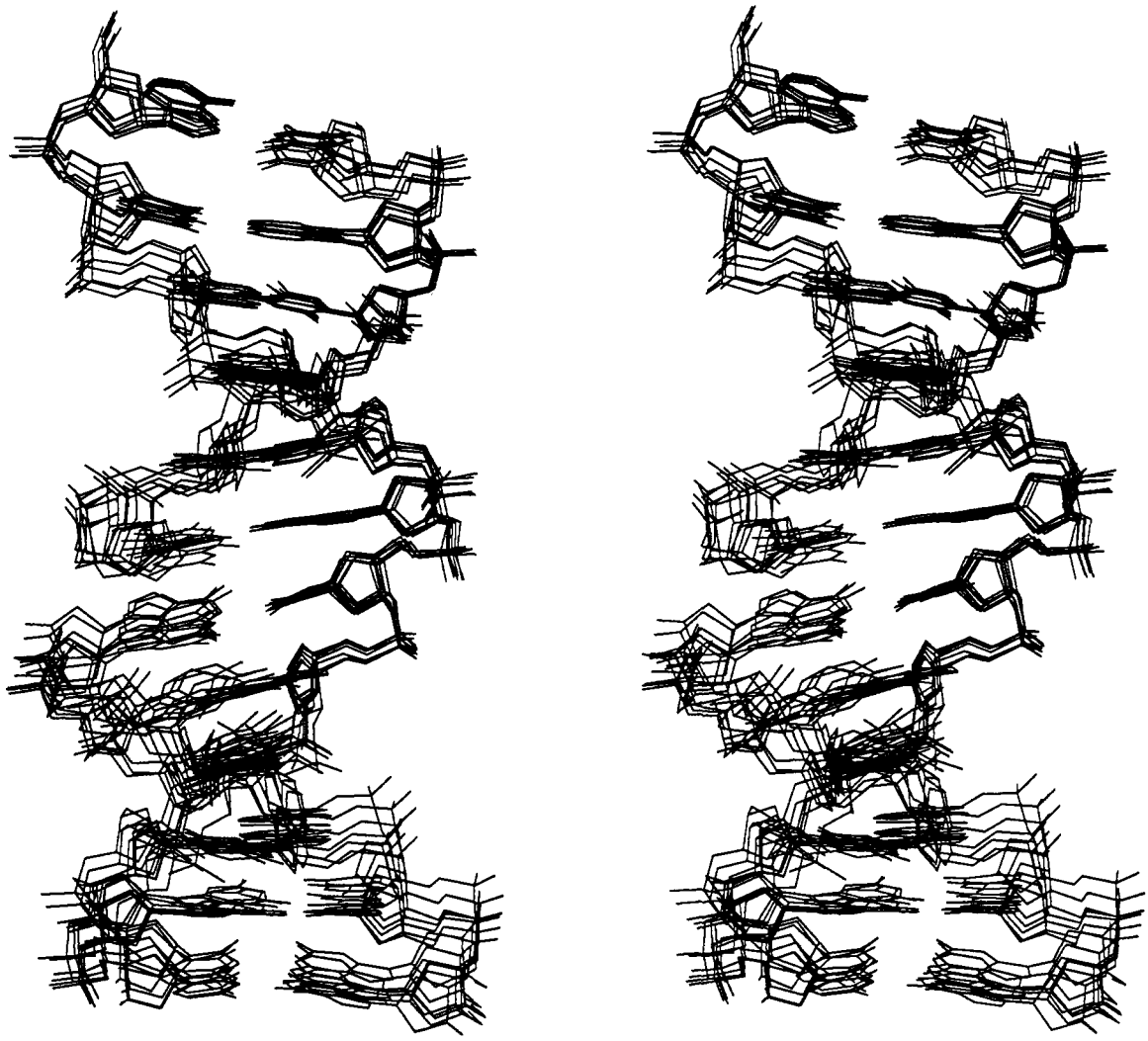

FIGURE 8: Stereoview of the superposition of stems I and III from the seven lowest energy solutions of J3CC. Hydrogen atoms are omitted for clarity. The view is into the minor groove of the colinear stems, with stem III on top. Residues T27 and T28 of the hairpin loop are not shown. Note the highly reproducible position of bases A34 and C35 on the right side of the molecule.

as well. It is possible that the G6(imino) proton resonance is broader and cannot be identified among the overlapping NOE cross peaks from other guanine imino protons. In our efforts to construct a model of the three-way junction, we have maintained all three of the internal base pairs. We feel this is a reasonable approach, since the NOE connectivities among the nonexchangeable protons of J3CC indicate that the helices are intact up to and including the junctional bases.

Three-Dimensional Model of the J3CC Junction. The new information from NOESY experiments in H_2O solution presented in this report, coupled with the assignments in D_2O discussed in the preceding paper, constitutes a framework for constructing a model of the three-way junction in solution. The formation of this model is based on the observed NOE connectivities, along with the assumption that the duplex arms of the junction may be represented as intact, B-form DNA helices. This assumption, which significantly reduces the complexity of the conformational search process, is based on our NMR results, as well as previous observations that the duplex arms of four-stranded DNA junctions exist in a B-like conformation (Marky et al., 1987; Chen et al., 1991).

We have completed a series of calculations, combining distance geometry and molecular dynamics, to obtain a number of structural models for the three-way DNA junction with two unpaired bases. Our results indicate that the informational content of our NOESY data does not permit us to choose a single conformation of the junction in solution. We therefore have presented our results as an envelope of conformations, within which certain structural features remain constant. Our inability to define the structure of the molecule in more detail is due to the limited amount and the qualitative nature of the information we were able to extract from the NOESY spectra. Our use of rigid helical stems to model the molecule structure of J3CC further necessitated this qualitative approach. As a consequence, our results are suggestive simply of the overall molecular conformation with regard to relative positioning of the helical and single-stranded regions of the molecule. We were able to define consistent structural features in our models, suggesting the importance of factors such as base stacking as determinants of the molecular conformation.

The most striking feature within the ensemble of solutions for the three-way DNA junction is the apparent colinearity between two of the three helices. This is the first direct demonstration of a pair-wise stacking interaction between helices within a multistranded DNA junction. Such interactions are thought to be important to the global conformation of multistranded junctions in both DNA and RNA. For example, in the presence of divalent metal ions, the four arms within synthetic Holliday junctions are thought to assume an "X" configuration, consisting of two pairs of stacked helices (Duckett et al., 1988; Cooper & Hagerman, 1989). Helical stacking is also evident in the three-dimensional structure of

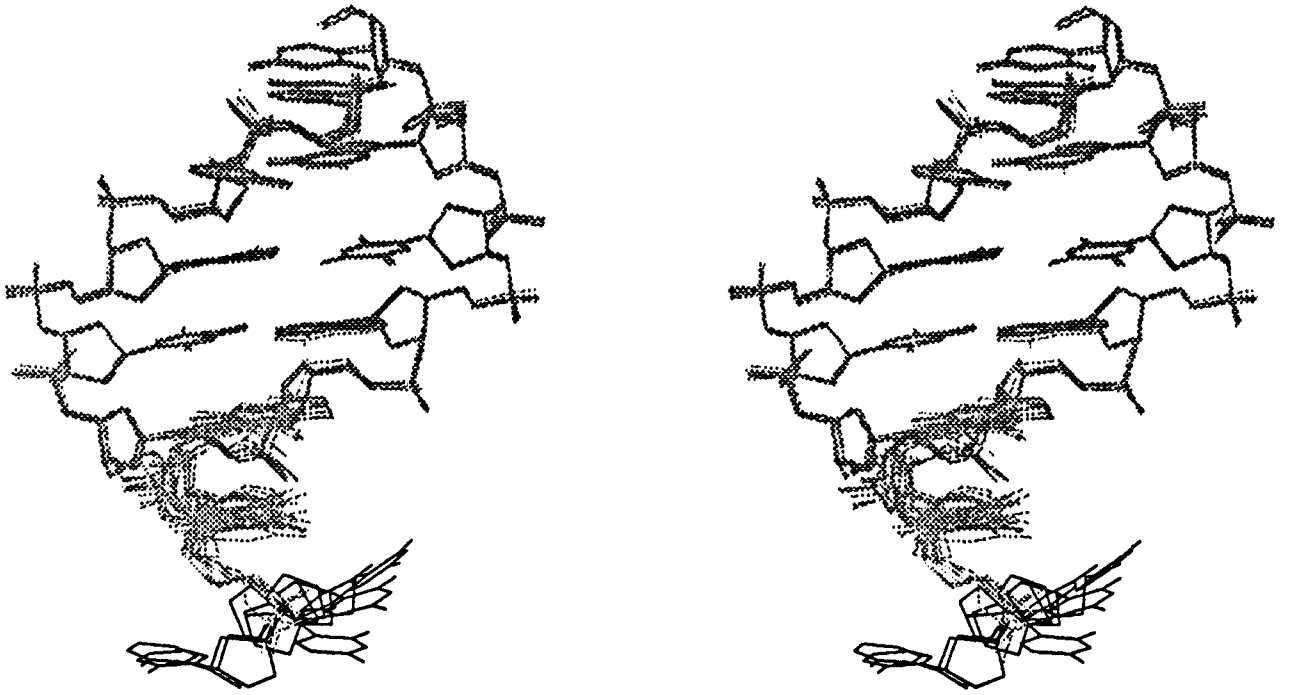

FIGURE 9: Stereoview of the superposition of stem II from the seven lowest energy solutions of J3CC. The variable position of the unpaired cytidine residue C8 at the base of the stem is highlighted. Hydrogen atoms are omitted for clarity.

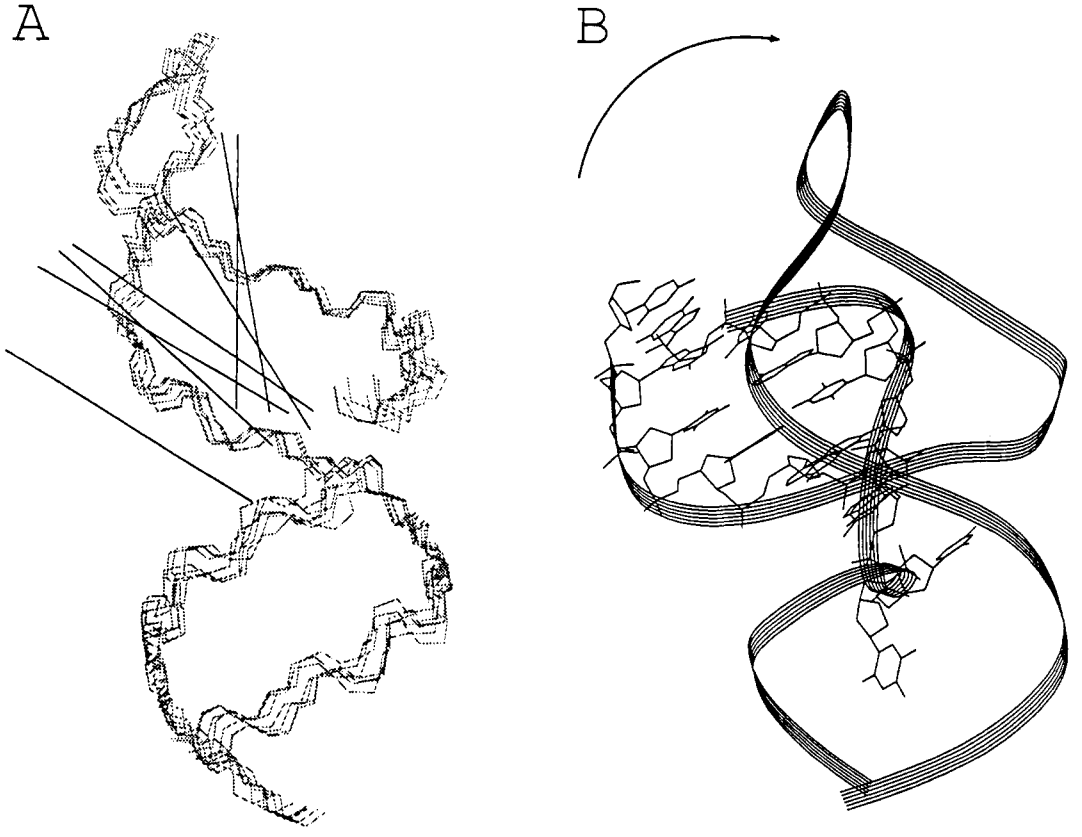

FIGURE 10: Side views of the junction models demonstrating the right-handed twist between stem II and the quasi-continuous helix from stems I and III. The view is rotated 90° from that of Figure 7. Stem II is located in front of the I–III colinear stack. (A) Superposition of the seven lowest energy structures. The sugar–phosphate backbones of stems I and III are shown, with the helical axes from stem II superimposed in front. The stem II–stem III angles in this projection range between 0° and 50°. (B) Side view of one junctional model, showing a stick diagram of stem II and the two unpaired cytidines against a ribbon representation of the entire molecule. The arrow indicates the direction of the twist angle.

tRNA (Kim et al., 1974). In another example, it has been suggested (Westhof et al., 1989; Brunel et al., 1991) that the three-way junction in the 5S RNA molecule can be modeled as a distorted "Y" structure in which two of the stems are partially stacked upon one another.

As was mentioned previously, the NOESY data in H_2O solution indicate that G9·C20 is the most stable of the three junctional base pairs. This result is somewhat surprising when one considers the tertiary structure of the molecule. The other junctional base pairs, G6·C35 and T21·A34, stack on one

another, whle G9·C20 is more solvent exposed. However, it is the base pairs which participate in stacking interactions across the branch point that are in fact less stable. This result suggests that these pairs are subject to a greater conformational stress than is the "freer" G9·C20 base pair. It is possible that, within the branch point region of J3CC, optimal base pair stacking can occur only through the partial destabilization of the participating Watson–Crick base pairs. Interestingly, this effect is more pronounced for G6·C35 than it is for T21·A34, suggesting that this stress is asymmetric with respect to the branch point geometry.

It is not clear at this time whether the preferred pair-wise stacking of stems I and III in the J3CC junction is directed by the base sequence at the branch point or by other geometric considerations. It has been shown (Duckett et al., 1988) that base sequence can direct the relative preference of stacking isomers in Holliday junctions. Furthermore, the presence of certain types of base pair mismatches at the branch point of these junctions has been shown to alter the global geometry of these molecules (Duckett & Lilley, 1991), as well as their drug-binding capabilities (Zhong et al., 1992). Base sequence at the branch point has also been found to influence the overall geometry in three-way DNA junctions (Lu et al., 1991). However, in asymmetric junctions such as J3CC, it is possible that stacking of helices within the junction is directed by geometric considerations alone. Certain gross conformational features of the J3CC model are replicated in control calculations performed without NOE restraints. It may be that, among the three possible combinations of pair-wise stacking of the helices in J3CC, the model in which stems I and III are colinear is the most sterically feasible. This hypothesis can be tested by examining the structure of variant three-way junctions in which the identity of the internal bases is altered.

Comparison between Structural Models of J3CC and the Three-Way Junction in the 5S RNA Molecule. Structural models of the 5S RNA molecule from *Escherichia coli*, *Xenopus laevis* oocyte, and spinach chloroplast have recently been proposed (Westhof et al., 1989; Brunel et al., 1991). These models are based on the accumulation of data from phylogenetic comparisons and chemical modification studies of native and mutant 5S RNA molecules. All of these 5S RNA molecules include a stretch of four unpaired bases in one strand at the branch point of the three-way junction. The structural models for these junctions feature a nearly colinear stack between two of the three helical stems. This configuration might be brought about in part through tertiary interactions involving these unpaired residues at the hinge region. In the *X. laevis* model, for example, a hydrogen bond between one of the unpaired bases, A13, and the G66·U109 wobble base pair at the beginning of helix D is proposed (Westhof et al., 1989). This interaction constrains the relative geometry of the helical stems.

In our previous study (Rosen & Patel, 1993), we contrasted the behavior of bulged pyrimidines and purines within three-way DNA junctions. Though we found no evidence for any tertiary hydrogen-bonding interactions involving the unpaired bases, we did note the unusual location of one unpaired cytidine base within the minor groove of the preceding helical stem. No such behavior was seen for either of the unpaired purine bases within the junctions studied. This difference in the behavior of bulged purine and pyrimidine bases at the branch point led to secondary changes in the overall geometry of the molecules.

Structural Models of Three- and Four-Way DNA Junctions. A model of the four-stranded Holliday junction has been proposed (von Kitzing et al., 1990), based on a comprehensive search for favorable alignments of the four helices at the junction. One energetically favorable alignment, thought to resemble the junction structure in the presence of divalent metal ions (Duckett et al., 1990), features two quasi-continuous helices in a noncrossed "X" configuration, oriented with a right-handed twist of approximately 60°. In our model for a three-way junction with unpaired bases, we also see a quasi-continuous helix formed from two of the stems. Furthermore, despite the greater range of conformations available to the three-way junction, our models consistently feature an acute angle (20–50°) between stems II and III of the junction. Among our models, energetic criteria clearly indicate a preference for junction geometries in which stem II and the I–III helix are related by a right-handed twist.

The acute angle between stems II and III in our models produces a sugar–phosphate backbone with an abrupt change in direction between bases C20 and T21. This conformational feature is analogous to the geometry of the exchanging strands within the Holliday junction model. Curiously, these two similar structural motifs are brought about by different backbone dihedral angle geometries. In the model of the Holliday junction, the backbone reorientation is due primarily to the conversion of the ϵ angle at the exchange point from the usual *trans* to a *gauche*$^-$ configuration, with a value of about −70°. Among our lowest energy models of J3CC, the ϵ angle between C20 and T21 migrates toward the *gauche*$^-$ configuration, ranging between −118° and −154° (mean value of −137°). However, the β dihedral of T21 completely reorients from the *trans* to the *gauche*$^-$ configuration, within a narrowly defined range of angles (between −77° and −95°). Von Kitzing and colleagues (1990) note that the *gauche*$^-$ arrangement of the ϵ dihedral angles from the two exchanging strands of the Holliday junction helps the molecule avoid unfavorable steric clash between phosphate groups from these opposing strands. In our three-way junction, there is only one "exchanging" strand and thus no steric conflict between phosphate groups across the branch point. This may explain the difference in the backbone geometries observed in the two studies.

The analogy between the three- and four-way DNA junctions also helps to explain the stabilizing effect of unpaired bases on three-way junctions. In nucleic acid duplexes, base pairing and base stacking contribute favorable free energy of complex formation, offsetting the unfavorable contribution from electrostatic repulsion. In the Holliday junction model, all four junctional Watson–Crick base pairs are intact, and two sets of base-stacking interactions are found spanning the branch point. This is illustrated schematically in Figure 11a. In J3CC, the disposition of the helical arms resembles that of a Holliday junction with one stem removed. Given this geometric arrangement, there is a large discontinuity in the sugar–phosphate backbone between two of the stems (Figure 11b). Among our models, the G6(O3′)–G9(P) distance ranges between 11.8 and 12.9 Å. The extended backbone of the two unpaired bases, C7 and C8, serves to bridge this gap (Figure 11c). However, in the absence of these bulged residues, the G6(O3′) and G9(P) atoms would be covalently bonded, necessitating a drastic reduction in the distance between these residues. The ensuing rearrangement of the helical stems could not occur without the disruption of either the Watson–Crick base pairing at the junction (Figure 11d) or the base stacking between helices I and III (Figure 11e). In either of these scenarios, the free energy of the system would increase due to the loss of energetically favorable stacking or pairing

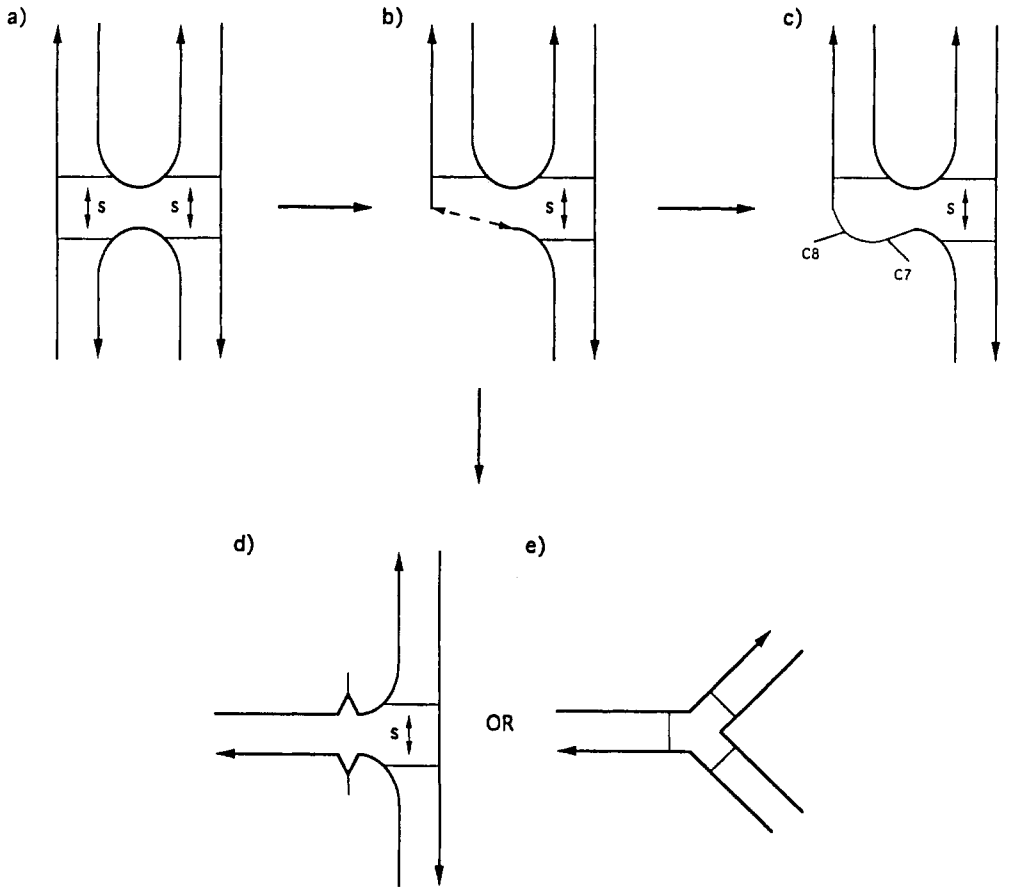

FIGURE 11: Schematic illustration of the stabilizing effect of unpaired bases at the branch point of three-way junctions. In (a), a four-way, Holliday junction is illustrated in the uncrossed-X configuration. The four junctional base pairs are shown as thin lines. Base pair stacking across the branch point is indicated by an "S". In (b), the removal of one stem of the Holliday junction results in a three-way junction. Retention of the uncrossed-X configuration within the remaining stems leaves a large gap in the sugar–phosphate backbone. (c) The addition of two unpaired bases (C7 and C8 in the J3CC junction) allows the molecule to retain the relative helical configuration by bridging the backbone discontinuity. Three internal base pairs and one base pair stacking interaction across the branch point are preserved. The positioning of bases C7 and C8 does not necessarily indicate their true position within the molecule. (d, e) Without the presence of the unpaired bases at the branch point, the helices of the three-way junction must reposition themselves, leading to disruption of either the internal base pairs or the base pair stacking interactions.

at the branch point. Furthermore, a reduction in the strength of the base-pairing or base-stacking interactions at the branch point would most likely result in a molecule with increased flexibility. This is precisely what has been observed for three-way DNA junctions lacking extra bases at the branch point (Ma et al., 1986). By bridging the long G6–G9 distance within the J3CC junction, the extended C7-C8 segment allows the helices to adopt the right-handed, uncrossed-X configuration, minus one helix.

Structural Determination of Complex Nucleic Acid Molecules from NMR Data. Nuclear magnetic resonance studies of nucleic acids in solution have been invaluable for investigating the structural properties of short DNA duplexes alone or in combination with exogenous ligands [for reviews, see Patel et al. (1987) and van de Ven and Hilbers (1988)]. Solution NMR studies have also shed light on the structure of unusual motifs such as bulge loops, mismatches, hairpins, and triplexes. For the most part, the thrust of these studies has been to elucidate conformational details at the local level. This is due for the most part to the fact that there is little tertiary structure in small nucleic acid molecules. However, as larger and more complicated systems containing multiple helices and junctions are studied, the elucidation of tertiary interactions becomes more critical to defining the three-dimensional structure of the molecule. In the absence of such information, NMR data alone cannot discriminate among the many possible configurational isomers.

Our results for the three-way DNA junction illustrate this difficulty. Despite a well-defined set of NOE restraints about the branch point of the junction, our simulations resulted in a wide range of geometric configurations of the molecule, most in apparent agreement with the NMR data. Energetic criteria were necessary in order to discriminate among the structural possibilities, allowing us to arrive at a single, well-defined envelope of structures describing the global positioning of the three helical stems in the molecule.

CONCLUSION

We have investigated the conformation and dynamics of a three-way DNA junction containing two unpaired cytidines at the branch point. NOESY experiments in H_2O establish a hierarchy of stabilities among the three internal Watson–Crick base pairs. One pair is intact at 20 °C, the second can be seen at a lower temperature (0 °C), and the third is either weakened or absent under these conditions. The first unpaired pyrimidine, C7, exhibits an unusual conformation in the junction. This base loops out from the interior of the molecule to lie within the minor groove of the preceding helical stem. The second bulged pyrimidine, C8, stacks under the G9·C20 pair at the base of stem II.

We have constructed models of the DNA junction consistent with the distance information derived from NOESY experiments in both D_2O and H_2O solutions. The helices are

arranged in a distorted Y configuration, with a preferred base-stacking interaction across the branch point. Two of the stems within the junction span an acute angle of 60° or less. In this configuration, the three-way junction resembles the proposed X model of the four-way Holliday junction with one of the four arms missing.

Our results suggest a mechanism for the stabilizing effect of unpaired bases in three-way junctions. The additional bases allow the molecule to adopt a geometry in which internal base pairing and base stacking are maximized. Without these additional bases, the covalent constraints at the branch point would prevent the molecule from simultaneously maximizing the number of Watson–Crick base pairs and maintaining base-stacking interactions across the branch point site.

ACKNOWLEDGMENT

We thank C. Hilbers (University of Nijmegen) for providing the coordinates of the TTTA hairpin loop structure and E. von Kitzing (Max Planck Institute) for the coordinates of the Holliday junction model. We also thank J. Hubbard for many helpful discussions regarding the use of distance geometry with nucleic acids and for critical reading of the manuscript.

SUPPLEMENTARY MATERIAL AVAILABLE

Four figures plotting the helicoidal parameters for the quasi-continuous helix (stems I and III) from the seven low-energy junction models (5 pages). Ordering information is given on any current masthead page.

REFERENCES

Baudin, F., Romaniuk, P. J., Romby, P., Brunel, C., Westhof, E., Ehresmann, B., & Ehresmann, C. (1991) *J. Mol. Biol. 218*, 69–81.

Blommers, M. J. J., Walter, J. A. L. I., Haasnoot, C. A. G., Aelen, J. M. A., van der Marel, G. A., von Boom, J. H., & Hilbers, C. W. (1989) *Biochemistry 28*, 7491–7498.

Blommers, M. J. J., van de Ven, F. J. M., van der Marel, G. A., van Boom, J. H., & Hilbers, C. W. (1991) *Eur. J. Biochem. 201*, 33–51.

Brunel, C., Romby, P., Westhof, E., Ehresmann, C., & Ehresmann, B. (1991) *J. Mol. Biol. 221*, 293–308.

Brunger, A. T. (1992) X-PLOR, Version 3.0, users manual, Yale University, New Haven, CT.

Chen, S.-M., Heffron, F., Leupin, W., & Chazin, W. J. (1991) *Biochemistry 30*, 766–771.

Chen, S.-M., Heffron, F., & Chazin, W. J. (1993) *Biochemistry 32*, 319–326.

Cooper, J. P., & Hagerman, P. J. (1989) *Proc. Natl. Acad. Sci. U.S.A. 86*, 7336–7340.

Duckett, D. R., & Lilley, D. M. J. (1990) *EMBO J. 9*, 1659–1664.

Duckett, D. R., & Lilley, D. M. J. (1991) *J. Mol. Biol. 221*, 147–161.

Duckett, D. R., Murchie, A. I. H., Diekmann, S., von Kitzing, E., Kemper, B., & Lilley, D. M. J. (1988) *Cell 55*, 79–89.

Duckett, D. R., Murchie, A. I. H., & Lilley, D. M. J. (1990) *EMBO J. 9*, 583–590.

Fasman, G. (1975) *CRC Handbook of Biochemistry and Molecular Biology*, 3rd ed., Vol. I, CRC Press, Inc., Boca Raton, FL.

Fox, J. W., & Woese, C. R. (1975) *Nature 256*, 505–506.

Hubbard, J. M., & Hearst, J. E. (1991) *Biochemistry 30*, 5458–5465.

Kim, S. H., Suddath, F. L., Quigley, G. J., McPherson, A., Sussman, J. L., Wang, A. H. J., Seeman, N. C., & Rich, A. (1974) *Science 185*, 435–440.

Kuszewski, J., Nilges, M., & Brunger, A. T. (1992) *J. Biomol. NMR 2*, 33–56.

Lavery, R., & Sklenar, H. (1988) *J. Biomol. Struct. Dyn. 6*, 63–91.

Lavery, R., & Sklenar, H. (1989) *J. Biomol. Struct. Dyn. 6*, 655–667.

Leontis, N. B., Kwok, W., & Newman, J. (1991) *Nucleic Acids Res. 19*, 759–766.

Lu, M., Guo, Q., & Kallenbach, N. R. (1991) *Biochemistry 30*, 5815–5820.

Ma, R.-I., Kallenbach, N. R., Sheardy, R. D., Petrillo, M. L., & Seeman, N. C. (1986) *Nucleic Acids Res. 14*, 9745–9753.

Marky, L. A., Kallenbach, N. R., McDonough, K. A., Seeman, N. C., & Breslauer, K. J. (1987) *Biopolymers 26*, 1621–1634.

Meselson, M. S., & Radding, C. H. (1975) *Proc. Natl. Acad. Sci. U.S.A. 72*, 358–361.

Nilsson, L., & Karplus, M. (1986) *J. Comput. Chem. 7*, 591–616.

Orr-Weaver, T. C., Szostak, J. W., & Rothstein, R. J. (1981) *Proc. Natl. Acad. Sci. U.S.A. 78*, 6354–6358.

Patel, D. J., Shapiro, L., & Hare, D. (1987) *Annu. Rev. Biophys. Biophys. Chem. 16*, 423–454.

Plateau, P., & Gueron, M. (1982) *J. Am. Chem. Soc. 104*, 7310–7311.

Ravishanker, G., Swaminathan, S., Beveridge, D. L., Lavery, R., & Sklenar, H. (1989) *J. Biomol. Struct. Dyn. 6*, 669–699.

Romaniuk, P. J. (1989) *Biochemistry 28*, 1388–1395.

Rosen, M. A., & Patel, D. J. (1993) *Biochemistry* (preceding paper in this issue).

Sigal, N., & Alberts, B. (1972) *J. Mol. Biol. 71*, 789–793.

States, D. J., Haberkorn, B. A., & Ruben, D. J. (1982) *J. Magn. Reson. 48*, 286–292.

van de Ven, F. J. M., & Hilbers, C. W. (1988) *Eur. J. Biochem. 178*, 1–38.

von Kitzing, E., Lilley, D. M. J., & Diekmann, S. (1990) *Nucleic Acids Res. 18*, 2671–2683.

Wemmer, D. E., Wand, A. J., Seeman, N. C., & Kallenbach, N. R. (1985) *Biochemistry 24*, 5745–5749.

Westhof, E., Romby, P., Romaniuk, P. J., Ebel, J.-P., Ehresmann, C., & Ehresmann, B. (1989) *J. Mol. Biol. 207*, 417–431.

Wolters, J., & Erdmann, V. A. (1988) *Nucleic Acids Res. 16* (Suppl.), r1–r70.

Zhong, M., Rashes, M. S., Marky, L. A., & Kallenbach, N. R. (1992) *Biochemistry 31*, 8064–8071.